Research article

Vincenzo Aglieri, Xin Jin, Andrea Rovere, Riccardo Piccoli, Diego Caraffini, Salvatore Tuccio, Francesco De Angelis, Roberto Morandotti, Roberto Macaluso, Andrea Toma* and Luca Razzari*

Improving nanoscale terahertz field localization by means of sharply tapered resonant nanoantennas

https://doi.org/10.1515/nanoph-2019-0459
Received November 6, 2019; revised December 6, 2019; accepted December 13, 2019

Abstract: Terahertz resonant nanoantennas have recently become a key tool to investigate otherwise inaccessible interactions of such long-wavelength radiation with nanomatter. Because of their high-aspect-ratio rod-shaped geometry, resonant nanoantennas suffer from severe loss, which ultimately limits their field localization performance. Here we show, via a quasi-analytical model, numerical simulations, and experimental evidence, that a proper tapering of such nanostructures relaxes their overall loss, leading to an augmented local field enhancement and a significantly reduced resonator mode volume. Our findings, which can also be extended to more complex geometries and higher frequencies, have profound implications for enhanced sensing and spectroscopy of nano-objects, as well as for designing more effective platforms for nanoscale long-wavelength cavity quantum electrodynamics.

Keywords: nanoantennas; terahertz science and technology; enhanced light-matter interaction.

***Corresponding authors: Andrea Toma,** Clean Room Facility, Istituto Italiano di Tecnologia, Via Morego 30, 16163, Genova, Italy, e-mail: Andrea.Toma@iit.it. https://orcid.org/0000-0003-2877-9805; and **Luca Razzari,** Institut National de la Recherche Scientifique – Énergie Matériaux et Télécommunications, 1650 Boulevard Lionel-Boulet, Varennes, Quebec, J3X 1S2, Canada, e-mail: razzari@emt.inrs.ca. https://orcid.org/0000-0002-8514-2192
Vincenzo Aglieri: Institut National de la Recherche Scientifique – Énergie Matériaux et Télécommunications, 1650 Boulevard Lionel-Boulet, Varennes, Quebec, J3X 1S2, Canada; Università degli Studi di Palermo – Dipartimento di Ingegneria, Viale delle Scienze, 90128, Palermo, Italy; and Istituto Italiano di Tecnologia, Via Morego 30, 16163, Genova, Italy. https://orcid.org/0000-0001-6274-7896
Xin Jin, Andrea Rovere, Riccardo Piccoli and Diego Caraffini: Institut National de la Recherche Scientifique – Énergie Matériaux et Télécommunications, 1650 Boulevard Lionel-Boulet, Varennes, Quebec, J3X 1S2, Canada. https://orcid.org/0000-0001-5858-6217 (X. Jin); https://orcid.org/0000-0002-5037-5471 (R. Piccoli)
Salvatore Tuccio and Francesco De Angelis: Istituto Italiano di Tecnologia, Via Morego 30, 16163, Genova, Italy. https://orcid.org/0000-0001-6053-2488 (F. De Angelis)
Roberto Morandotti: Institut National de la Recherche Scientifique – Énergie Matériaux et Télécommunications, 1650 Boulevard Lionel-Boulet, Varennes, Quebec, J3X 1S2, Canada; and IFFS, University of Electronic Science and Technology of China, Chengdu, 610054 Sichuan, China. (Adjoint Faculty). https://orcid.org/0000-0001-7717-1519
Roberto Macaluso: Università degli Studi di Palermo – Dipartimento di Ingegneria, Viale delle Scienze, 90128, Palermo, Italy. https://orcid.org/0000-0002-7612-3192

1 Introduction

Following the fast advances in nanofabrication technologies during the last decade, plasmonic nanoantennas (NAs) have quickly become a hectic research field, driven by the distinctive capability of such devices to convert free-propagating radiation into strongly localized electric/magnetic fields beyond the diffraction limit [1]. This is made possible by the excitation of surface (plasmonic) modes at the interface between the metallic antenna and the surrounding environment [2]. Two key parameters are generally considered for describing the localization performance of NAs, i.e. the near-field enhancement factor (the ratio of the local field to the free-space field) and the mode volume (the effective volume occupied by the radiation in the NA surroundings). High near-field enhancement factors within extremely sub-wavelength mode volumes have proven to effectively boost light-matter interactions by orders of magnitude [1, 3]. High local fields have been used for, e.g. single-molecule imaging [4], sensing of electrochemical processes [5], enhanced infrared, Raman, and terahertz (THz) spectroscopies [6–9], as well as enhanced nonlinear phenomena [10], while extremely small mode volumes have been directly exploited in strong coupling experiments [11, 12], since the light-matter coupling strength scales with the inverse square root of such quantity.

The THz frequency domain (~0.1–10 THz) hosts several low-energy excitations, such as phonons,

magnons, and intra-excitonic transitions [13], being thus extremely attractive to investigate a vast variety of fundamental light-matter interactions. However, the intrinsic long wavelength associated with THz radiation (~300 μm at 1 THz), typically hampers the use of THz waves for the investigation of nano-systems. In this context, NAs have proven to be a valuable tool to overcome the difficulty to sense nano-objects and very low amounts of chemical compounds in standard THz far-field spectroscopy [14]. Indeed, they have been successfully employed for small molecules [15, 16] and microorganism detection [17], for enhanced THz spectroscopy [9, 18], and, more recently, for demonstrating nanoscale vibrational (phonon) strong coupling [11]. A straightforward strategy to make long-wavelength THz waves interact with a single or a few nano-objects would consist in drastically decreasing the lateral cross-sectional area of a standard rod-like NA. However, this is known to cause a significant increase in the Ohmic loss that the surface mode experiences on the metal interface [19], which becomes critical for resonant THz NAs due to the extreme mismatch between their lateral cross-section and the radiation wavelength. Consequently, the capacity to efficiently convert free-space radiation into sub-wavelength localized hot spots is severely affected in the THz regime. In order to improve the field localization, nano-gaps between end-to-end-coupled NAs (instead of single antennas) have been proposed, which can further squeeze the local field in reduced volumes by shrinking the gap width. However, such a drastic reduction in width eventually results in electron tunneling across the gap, which ultimately limits the field concentration [20]. Alternative geometries have also been proposed for improving the near-field enhancement over a wide span of frequency ranges. For instance, semi-infinite tapered waveguides have been theoretically shown to increase the plasmonic energy density at the waveguide tip of more than 20 times [21], and nonresonant tapered gold rods have been numerically demonstrated to produce stronger near fields as a result of the optimal tapering design [22, 23]. These geometries have indeed attracted great attention for their ability to strongly focus the electromagnetic field at their smaller end [1, 21], which makes them a valuable choice for, e.g. nanoscale imaging and spectroscopy [24]. Tapered resonant structures, in the form of single or coupled (popularized as "bow-tie" [25]) antennas, have also been extensively studied [25–28]. In the visible/infrared domains, it was, however, commonly reported that the larger the tapering angle, the smaller the near-field enhancement [28–32]. In this article, we show that a proper tapering of THz NAs can effectively minimize the nanoresonator loss, leading to improved field localization and enhancement. Specifically, we present a simplified quasi-analytical model to study the NA performance as a function of the tapering angle. The NA is described as a Fabry-Perot resonator [33], taking into account not only the Ohmic effects within the metal (nonradiative loss) but also the loss related to the radiation coupling into free space at the antenna extremities (radiative loss). Such a model reveals the existence of a tradeoff (i.e. an optimum tapering angle) between a reduced nonradiative loss for large angles and a corresponding increased radiative loss, associated with a drop in the reflection coefficient for the surface mode at the enlarged antenna extremity. This behavior is then confirmed in a planar bow-tie geometry by means of numerical simulations (COMSOL Multiphysics). Such study reveals a ~2.2-fold increase in near-field enhancement and a 7-fold reduction in mode volume for optimally tapered NA pairs resonating at around 1 THz with a lateral cross-sectional area of 60×100 nm^2 at the gap (gap width 30 nm). We finally fabricated these nanostructures and characterized them via far-field THz spectroscopy, establishing the ability of our tapering strategy to significantly reduce the overall resonator loss.

2 Principle and design of THz tapered nanoantennas

In order to get a physical insight into the mechanism that gives rise to the optical response of tapered NAs, we developed a quasi-analytical model exploiting a Fabry-Perot resonator analogy for the NA surface mode [14, 33, 34]. In this simplified model, we consider the fundamental TM_0 mode excited on a gold NA of cylindrical symmetry (for calculation simplicity) with radius $r(z)$ (z being the coordinate along the NA length), length L, and THz permittivity ϵ_m as in Ref. [35]. In this way, the complex effective refractive index $n_{\text{eff}}(z)$ of the NA can be readily calculated from the relation $(\epsilon_m/\kappa_m)((I_1(\psi_m r))/(I_0(\psi_m r)) + (\epsilon_d/\kappa_d)(K_1(\psi_d r))/(K_0(\psi_d r)) = 0$, where ϵ_m and ϵ_d are the permittivity of the metal and surrounding dielectric, respectively, I_j and K_j ($j = 0,1$) are the modified Bessel functions, $\psi_{m,d} = \kappa_0 \sqrt{(n_{\text{eff}}^2 - \epsilon_{m,d})}$, $\kappa_0 = \omega/c$ (with ω the angular frequency and c the speed of light in vacuum), and $\kappa_{m,d} = \sqrt{(n_{\text{eff}}^2 - \epsilon_{m,d})}$ [14, 36, 37]. We can envision the excited surface mode as propagating back and forth along the NA and being reflected at each half round-trip at the NA extremities, so that a standing wave is formed at a specific wavelength [$\lambda_{\text{res}} \cong 2n_{\text{eff}} L$ for the first (dipolar) resonance of a cylinder with fixed radius [14]], which represents the NA resonance. The reflection coefficients can be calculated by

matching, at the NA ends, the transverse electric and magnetic components of the surface wave with the free-space modes, as reported in detail in Ref. [37]. Finally, the electric field at the resonator extremity is retrieved following the traditional procedure used for a Fabry-Perot cavity:

$$E_{\text{tip}} = E_0 \frac{(1-Re^{2j\phi})(1-e^{2j\phi})}{1-RR_\theta e^{4j\phi}}, \quad (1)$$

where R and R_θ are the reflection coefficients at the tip and at the larger extremity, respectively, E_0 is a reference input value for the surface wave electric field, and $\phi = \kappa_0 \int_0^L n_{\text{eff}}(z)\text{d}z$ is the complex phase accumulated in a half round trip by the surface mode over the antenna [14, 38].

The tapered geometry is taken into account considering the NA as a truncated cone (see Figure 1A) with tapering angle θ, length $L = 100$ µm, and tip radius 50 nm, which results in a dipolar resonance at approximately 1 THz. The effective index n_{eff} varies along the structure as a consequence of its dependence on the local radius, $r' = r + z \tan(\theta)$, with $0 < z < L$. Figure 1B (bottom) shows the tip electric field at resonance (orange curve), calculated using Eq. (1), as a function of the tapering angle θ. As one can see, for small θ values, this field increases as the angle increases. Then, after a maximum value is reached, the tip field starts decreasing for larger θ values. The presence of a maximum in the tip field behavior can be explained as a tradeoff between the radiative resonator loss, related to the reflection coefficients at the antenna extremities, and the nonradiative (Ohmic) loss. Indeed, for large NA local radii, the imaginary part of the effective index n_{eff} decreases, leading to a lower nonradiative loss for the surface mode when θ is increased. However, at the same time, the reflection coefficient at the larger extremity decreases significantly for large angles, resulting in higher radiative loss (i.e. coupling to the free-space modes). This tradeoff can be visualized by plotting the total normalized resonator power loss per round trip $P_{\text{loss}} = 1 - \gamma_r \gamma_{\text{nr}}$ (dark gray curves in Figure 1B, which reveal a minimum corresponding to the optimum tapering angle), as well as the terms that separately account for the radiative and nonradiative contributions to the total loss [$\gamma_r = R^2 R_\theta^2$ and $\gamma_{\text{nr}} = e^{-4\kappa_0 \int_0^L \text{Im}\{n_{\text{eff}}(z)\}\text{d}z}$, red and blue curve, respectively, in Figure 1B; notice that $\gamma_r = 1$ ($\gamma_{\text{nr}} = 1$) for no radiative (no nonradiative) loss]. Summarizing, a careful choice of the tapering angle can minimize the overall loss of the NA

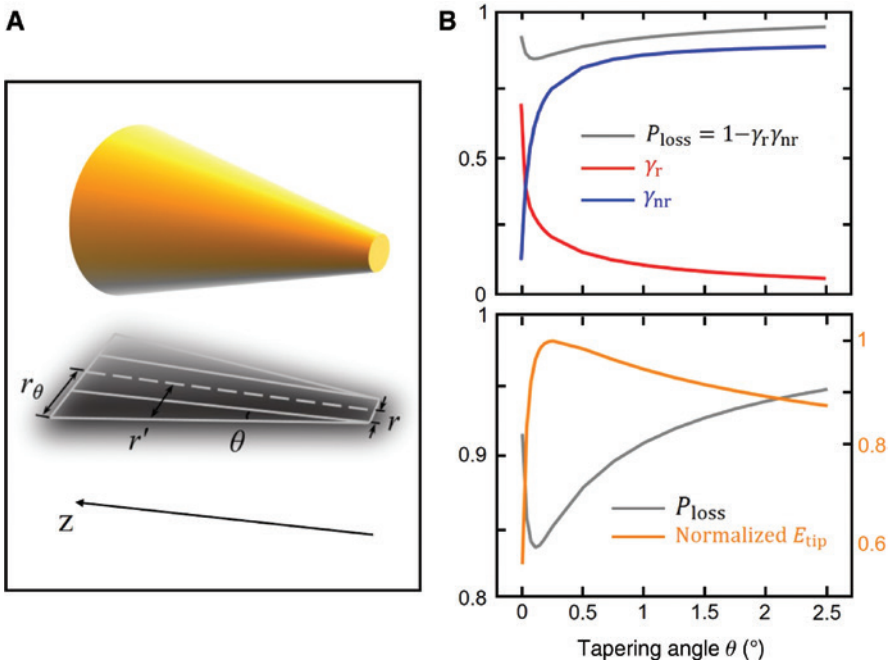

Figure 1: Quasi-analytical model.
(A) Sketch of a tapered NA, with r, r_θ, and r' being the radius of the smaller extremity (fixed at 50 nm), radius of the larger end, and the local radius at a specific z, respectively. (B) Top: quantity γ_r related to the radiative loss (red), quantity γ_{nr} related to the nonradiative loss (blue), and the total normalized power loss per round trip $P_{\text{loss}} = 1 - \gamma_r \gamma_{\text{nr}}$, revealing a minimum for an optimum angle (dark gray). Bottom: the normalized absolute value of the tip field amplitude at the resonance frequency ($f_{\text{res}} = 1.1$ THz) as a function of the tapering angle θ (orange), calculated using the Fabry-Perot model. P_{loss} is once again shown to highlight its correlation with the local field trend (dark gray).

resonator, thus improving the local field enhancement at the tip.

While this model gives an intuitive picture of the proposed tapering approach, to investigate the optical behavior of a more realistic geometry that can be fabricated using conventional processes (specifically, a resonant planar NA dimer [39]), we performed extensive 3D numerical simulations. In particular, we studied bow-tie NA pairs (separated by a 30-nm-wide gap) over a silicon substrate. Such system was designed to resonate at around 1 THz and to present an overdamped response in its rod-like configuration ($\theta = 0°$), in order to clearly highlight the beneficial effects of the NA tapering. In particular, each gold NA of the dimer is 45 μm long, 60 nm thick, and 100 nm wide (at the nanogap). Figure 2A shows a 2D color map of the near-field enhancement (calculated at the center of the gap) as a function of both the frequency and tapering angle. As can be observed, by slightly increasing the tapering angle, a pronounced resonance appears, featuring a larger field enhancement (dark red area in Figure 2A) when compared to the rod-like geometry, as also predicted by the quasi-analytical model. Figure 2B tracks the trend of the local field enhancement at resonance (main figure) and of the resonance frequency (inset) as a function of θ. The largest enhancements are observed in the region $\theta = 3$–$5°$, with values ~2.2 times higher than the rod-shaped NA case ($\theta = 0°$). It is worth underlining that the nontapered NA response, due to overdamping, does not feature a resonance adjustable via NA length tuning, and the field enhancement value we considered for the above comparison (plotted as a red square in Figure 2B) has its origin in the so-called lightning-rod effect [40]. The latter is always present on structures with a small radius of curvature, being large for long wavelengths. Thus, the field enhancement comparison does not fully express the improved performance of the tapered NAs. The significant red shift of the near-field enhancement resonance observed for $\theta < 2.5°$ (inset of Figure 2B) is a well-known effect in THz NAs featuring severe losses [19]. Figure 2C–H additionally shows the 2D spatial maps of the near-field distribution in the gap region at resonance for some of the simulated tapering angles, further highlighting the improved field localization and boost via NA tapering. Numerical simulations also give access to another important parameter to evaluate the electric field localization, i.e. the NA mode volume, which is defined as $V_{\mathrm{mod}} = \int \epsilon(r)|E(r)|^2 \mathrm{d}r / \max(\epsilon(r)|E(r)|^2)$ [41], where ϵ is the dielectric permittivity and E is the electric field at the point r, the integral being calculated in a volume comprising the whole NA structure. This quantity is of fundamental importance in strong coupling experiments since, as mentioned earlier, an extremely small mode volume guarantees a large coupling strength [42]. In Figure 3B, we map the ratio of the mode volume to the fixed geometric

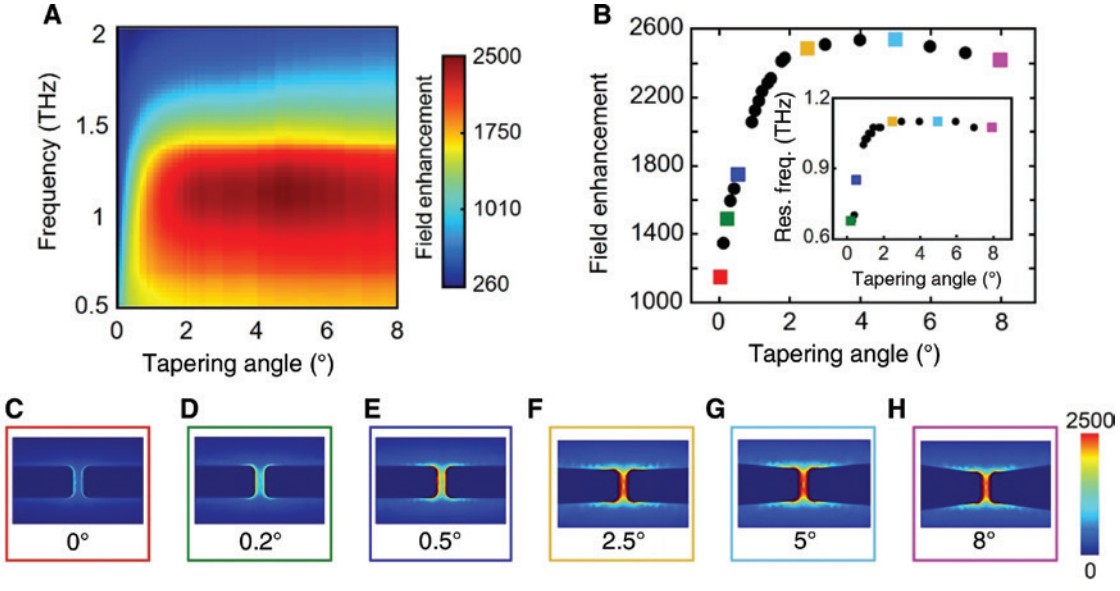

Figure 2: Numerical simulations – field enhancement.
(A) Near-field enhancement in the center of the gap as a function of frequency and tapering angle. (B) Near-field enhancement at resonance as a function of the tapering angle. The inset shows the corresponding shift of the resonance frequency with the tapering angle. (C–H) Local electric field amplitude maps of the nanogap area for selected tapering angles at resonance ($f = 0.5$ THz for the 0° case). All data were obtained via COMSOL simulations.

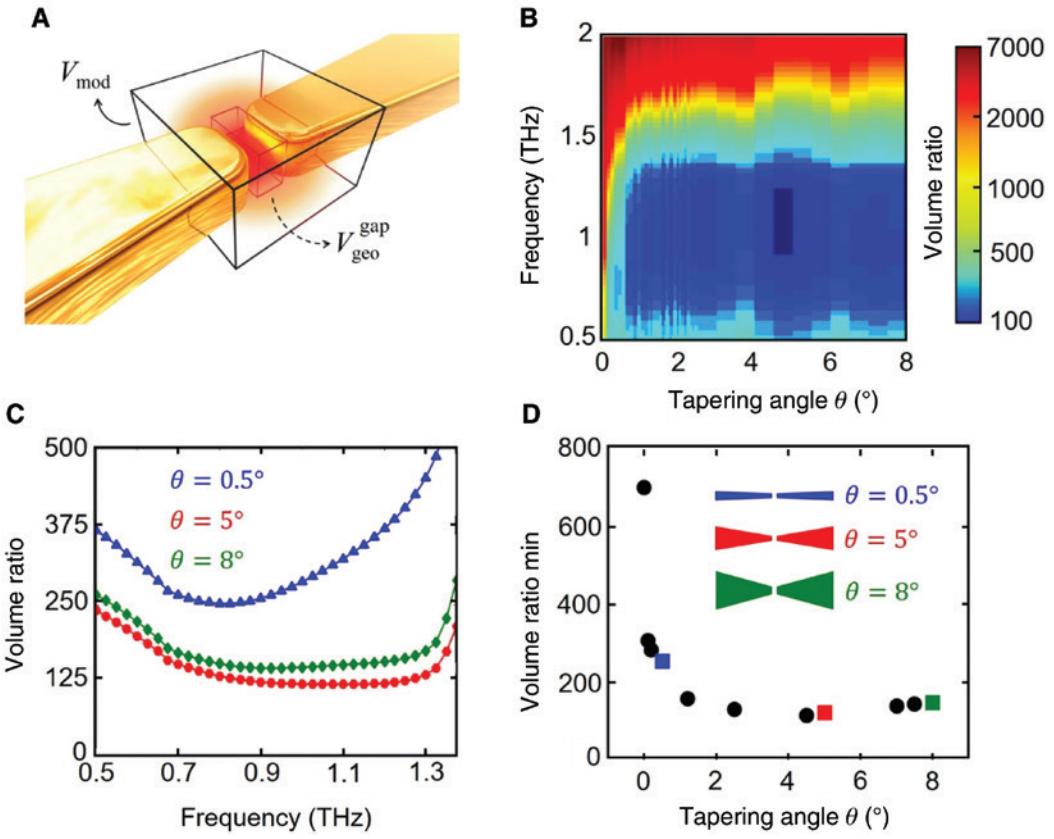

Figure 3: Numerical simulations – mode volume.
(A) Sketch of the NA dimer, highlighting the mode volume V_{mod} and the geometrical volume of the gap V_{geo}^{gap}. (B) Volume ratio ($V_{ratio} = V_{mod}/V_{geo}^{gap}$) plotted as a function of frequency and tapering angle. (C) Volume ratio as a function of frequency for three representative bow-tie tapering angles: $\theta = 0.5°$ (blue), 5° (red), and 8° (green). (D) Volume ratio minima (at resonance, $f = 0.5$ THz for the 0° case) as a function of the tapering angle.

volume V_{geo}^{gap} of the nanogap (i.e. $30 \times 60 \times 100$ nm^3, see sketch in Figure 3A) as a function of both the frequency and the tapering angle. Following a behavior similar to the one observed for the field enhancement (Figure 2A), even the mode volume reduction is found to be drastically improved by increasing the tapering angle, reaching a plateau for $\theta > 2°$ with values slightly over 100 times V_{geo}^{gap} at resonance (Figure 3C,D), attaining approximately a 7-fold reduction with respect to the rod-shaped case. It is worth stressing that these are remarkably small values, especially considering that the overall geometrical volume of the NA dimer (V_{geo}^{tot}) increases significantly by widening the tapering angle (going from 3000 to ~190,000 times V_{geo}^{gap}, when increasing θ from 0° to 8°). In brief, through a proper tailoring of THz resonant NAs, we envision the possibility of significantly improving their field enhancement and mode volume performance, opening intriguing perspectives in light-nanomatter interaction at low energies, with straightforward applications in, e.g. sensing of individual nano-objects.

3 Tapered NAs: fabrication and characterization

In order to experimentally validate our strategy, we fabricated five samples of NA dimer arrays with tapering angles $\theta = 0°$, 0.2°, 0.5°, 2.5°, and 5° (antenna height, length, and width, as well as gap size, were fixed to the values used in our numerical simulations). The nanostructures were prepared on top of a high-resistivity silicon substrate (10,000 Ω · cm), which provides both negligible loss and chromatic dispersion at THz frequencies. Figure 4A shows a representative scanning electron microscope (SEM) micrograph of the array of gold dimers featuring $\theta = 5°$, while details of the gap region are shown in the insets.

Fabrication was performed via electron beam lithography, and the samples were characterized by means of THz time-domain spectroscopy (TDS) in transmission configuration (see Supporting Information). As expected, an increase in the tapering angle gives rise to a clear

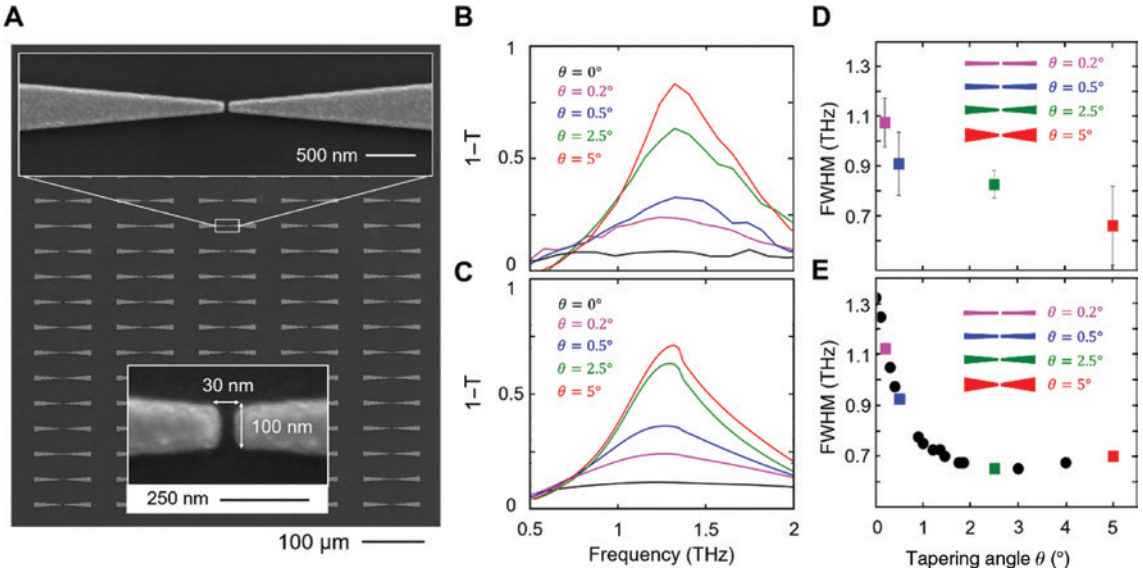

Figure 4: Experimental validation.
(A) Scanning electron micrograph of the gold NA dimer array with $\theta = 5°$. The insets show further details of a tapered NA dimer (top) and a zoom of the gap area down to the nanometer scale (bottom). (B, C) Experimental (1–*T*) spectra of the fabricated samples (*T* is the normalized transmission; the normalization is performed using the transmission of a bare silicon substrate; the quantity 1–*T* is sometimes referred to as extinction [43]) and the corresponding simulated spectra, respectively. (D, E) FWHM values of the experimental and simulated spectral response, respectively.

resonance formation in the spectral response (Figure 4B). In order to achieve reliable experimental evidence for the fact that NA tapering leads to reduced loss, as predicted by both our quasi-analytical model and numerical simulations, we then extracted the resonance full width at half-maximum (FWHM) for the various arrays (Figure 4D). Indeed, this parameter is a direct indicator of the total loss (radiative and nonradiative) in a resonator [44]. An evident decrease in FWHM is observed in the experimental spectra for the tapered NA dimer arrays, thus confirming the reduction in loss. No meaningful FWHM value could be extracted for $\theta = 0°$, as in this case, by design, the resonance is significantly overdamped. Finally, the corresponding simulated spectral response and related FWHM values (Figure 4C–E) confirm the reported trend, in agreement with the experimental results.

4 Conclusion

We have shown that by properly tapering NAs resonating in the THz frequency range, a significant boost in the electric field localization performance of such devices can be achieved. We first developed a simplified quasi-analytical model that demonstrated the existence of an optimum tapering angle capable of minimizing the overall resonator loss and thus improving the local field enhancement. This behavior was confirmed by extensive numerical simulations on planar nanostructures (NA dimers), which also returned quantitative information regarding the mode volume reduction by means of tapering. In particular, for the specific geometry considered, our study revealed a 2.2-fold increase in the near-field enhancement and a 7-fold decrease in mode volume when optimally tapered structures were compared with straight NA dimers (the latter featuring an overdamped, nontunable spectral response). Finally, we fabricated five NA dimer samples with different tapering angles and characterized their THz response by means of transmission spectroscopy. The so-obtained experimental spectra confirmed a significant reduction of the resonance FWHM via tapering, a distinctive signature of the reduction of the resonator loss. Our findings are significant for improving light-nanomatter interaction at low frequencies, with direct implications for those applications in which the effective localization of the THz electric field plays a central role, such as sensing, enhanced spectroscopy, and strong coupling experiments. While the proposed strategy was tested on simplified structures with fixed tapering angles, it can also be extended to more complex geometries. For example, one can envision the design of “shuttle” (rhomboidal) antennas, which would still allow reducing the resonator loss via tapering while maintaining two “hot spots” at their extremities. In addition, although we have validated our

approach at THz frequencies, we underline the fact that it represents a general route to improving the field localization performance of high-aspect-ratio NAs, even at higher frequencies, as demonstrated by our further simulations of tapered NA dimers resonating in the infrared (see Supporting Information).

Acknowledgments: LR and RM are grateful for financial support from the Natural Sciences and Engineering Research Council of Canada (NSERC) through the Strategic and Discovery grant programs. RM acknowledges additional support from the Canada Research Chair Program. VA and XJ are grateful for support from NSERC CREATE: Guided Light. XJ would also like to thank the Fonds de Recherche du Québec – Nature et Technologies (FRQNT) for a Doctoral Research Scholarship: Programme de Bourse d'Excellence pour Étudiants Étrangers (PBEEE – V1).

References

[1] Biagioni P, Huang J-S, Hecht B. Nanoantennas for visible and infrared radiation. Rep Prog Phys 2012;75:024402.
[2] Maier SA. Plasmonics: fundamentals and applications. Berlin, NY: Springer US, 2007.
[3] Bharadwaj P, Deutsch B, Novotny L. Optical antennas. Adv Opt Photon 2009;1:438.
[4] Taminiau TH, Moerland RJ, Segerink FB, Kuipers L, van Hulst NF. $\lambda/4$ resonance of an optical monopole antenna probed by single molecule fluorescence. Nano Lett 2007;7:28–33.
[5] Hoener BS, Kirchner SR, Heiderscheit TS, et al. Plasmonic sensing and control of single-nanoparticle electrochemistry. Chem 2018;4:1560–85.
[6] D'Andrea C, Bochterle J, Toma A, et al. Optical nanoantennas for multiband surface-enhanced infrared and Raman spectroscopy. ACS Nano 2013;7:3522–31.
[7] Ding S-Y, Yi J, Li J-F, et al. Nanostructure-based plasmon-enhanced Raman spectroscopy for surface analysis of materials. Nat Rev Mater 2016;1:1–16.
[8] Abb M, Wang Y, Papasimakis N, de Groot CH, Muskens OL. Surface-enhanced infrared spectroscopy using metal oxide plasmonic antenna arrays. Nano Lett 2014;14:346–52.
[9] Toma A, Tuccio S, Prato M, et al. Squeezing terahertz light into nanovolumes: nanoantenna enhanced terahertz spectroscopy (NETS) of semiconductor quantum dots. Nano Lett 2015;15:386–91.
[10] Kauranen M, Zayats AV. Nonlinear plasmonics. Nat Photon 2012;6:737–48.
[11] Jin X, Cerea A, Messina GC, et al. Reshaping the phonon energy landscape of nanocrystals inside a terahertz plasmonic nanocavity. Nat Commun 2018;9:763.
[12] Törmä P, Barnes WL. Strong coupling between surface plasmon polaritons and emitters: a review. Rep Prog Phys 2014;78:013901.
[13] Dexheimer SL. Terahertz spectroscopy: principles and applications. Boca Raton, FL, CRC Press, 2007.
[14] Piccoli R, Rovere A, Toma A, Morandotti R, Razzari L. Terahertz nanoantennas for enhanced spectroscopy. In: Uddin J, editor. Terahertz spectroscopy – a cutting edge technology. London, UK, InTech, 2017.
[15] Park H-R, Ahn KJ, Han S, Bahk Y-M, Park N, Kim D-S. Colossal absorption of molecules inside single terahertz nanoantennas. Nano Lett 2013;13:1782–6.
[16] Lee D-K, Kang J-H, Lee J-S, et al. Highly sensitive and selective sugar detection by terahertz nano-antennas. Sci Rep 2015;5:15459.
[17] Park SJ, Hong JT, Choi SJ, et al. Detection of microorganisms using terahertz metamaterials. Sci Rep 2014;4:4988.
[18] Ueno K, Nozawa S, Misawa H. Surface-enhanced terahertz spectroscopy using gold rod structures resonant with terahertz waves. Opt Express 2015;23:28584.
[19] Sarid D, Challener W. Modern introduction to surface plasmons: theory, mathematica modeling and applications. Cambridge: Cambridge University Press, 2010.
[20] Zuloaga J, Prodan E, Nordlander P. Quantum description of the plasmon resonances of a nanoparticle dimer. Nano Lett 2009;9:887–91.
[21] Pile DFP, Gramotnev DK. Adiabatic and nonadiabatic nanofocusing of plasmons by tapered gap plasmon waveguides. Appl Phys Lett 2006;89:041111.
[22] Gramotnev DK, Vogel MW, Stockman MI. Optimized nonadiabatic nanofocusing of plasmons by tapered metal rods. J Appl Phys 2008;104:034311.
[23] Thomas S, Wachter G, Lemell C, Burgdörfer J, Hommelhoff P. Large optical field enhancement for nanotips with large opening angles. New J Phys 2015;17:063010.
[24] Kawata S. Near-field optics and surface plasmon polaritons. Topics in applied physics. Berlin, NY: Springer, 2001.
[25] Schuck PJ, Fromm DP, Sundaramurthy A, Kino GS, Moerner WE. Improving the mismatch between light and nanoscale objects with gold bowtie nanoantennas. Phys Rev Lett 2005;94:017402.
[26] Hao E, Schatz GC. Electromagnetic fields around silver nanoparticles and dimers. J Chem Phys 2004;120:357–66.
[27] Farahani JN, Pohl DW, Eisler H-J, Hecht B. Single quantum dot coupled to a scanning optical antenna: a tunable superemitter. Phys Rev Lett 2005;95:017402.
[28] Crozier KB, Sundaramurthy A, Kino GS, Quate CF. Optical antennas: resonators for local field enhancement. J Appl Phys 2003;94:4632–42.
[29] Yang J, Kong F, Li K, Zhao J. Optimizing the Bowtie nanoantenna for enhanced Purcell factor and electric field. Prog Electromagn Res Lett 2014;44:93–9.
[30] Bi G, Wang L, Ling L, et al. Optical properties of gold nano-Bowtie structures. Opt Commun 2013;294:213–7.
[31] Lee C-H, Liao S-C, Lin T-R. Boosted photocatalytic efficiency through plasmonic field confinement with Bowtie and Diabolo nanostructures under LED irradiation. Opt Express 2016;24:17541.
[32] Fischer H, Martin OJF. Engineering the optical response of plasmonic nanoantennas. Opt Express 2008;16:9144.
[33] Cubukcu E, Capasso F. Optical nanorod antennas as dispersive one-dimensional Fabry–Pérot resonators for surface plasmons. Appl Phys Lett 2009;95:201101.
[34] Tuccio S, Razzari L, Alabastri A, et al. Direct determination of the resonance properties of metallic conical nanoantennas. Opt Lett 2014;39:571.

[35] Walther M, Cooke DG, Sherstan C, Hajar M, Freeman MR, Hegmann FA. Terahertz conductivity of thin gold films at the metal-insulator percolation transition. Phys Rev B 2007;76:125408.
[36] Babadjanyan AJ, Margaryan NL, Nerkararyan KV. Superfocusing of surface polaritons in the conical structure. J Appl Phys 2000;87:3785–8.
[37] Gordon R. Reflection of cylindrical surface waves. Opt Express 2009;17:18621–9.
[38] Stockman MI. Nanofocusing of optical energy in tapered plasmonic waveguides. Phys Rev Lett 2004;93:137404.
[39] Razzari L, Toma A, Clerici M, et al. Terahertz dipole nanoantenna arrays: resonance characteristics. Plasmonics 2013;8:133–8.
[40] Zhang W, Cui X, Martin OJF. Local field enhancement of an infinite conical metal tip illuminated by a focused beam. J Raman Spectrosc 2009;40:1338–42.
[41] Koenderink AF. On the use of Purcell factors for plasmon antennas. Opt Lett 2010;35:4208.
[42] Yang Z-J, Antosiewicz TJ, Shegai T. Role of material loss and mode volume of plasmonic nanocavities for strong plasmon-exciton interactions. Opt Express 2016;24:20373.
[43] Kats MA, Genevet P, Aoust G, Yu N, Blanchard R, Aieta F, et al. Giant birefringence in optical antenna arrays with widely tailorable optical anisotropy. PNAS 2012;109:12364–8.
[44] Ismail N, Kores CC, Geskus D, Pollnau M. Fabry-Pérot resonator: spectral line shapes, generic and related airy distributions, linewidths, finesses, and performance at low or frequency-dependent reflectivity. Opt Express 2016;24:16366.

Supplementary Material: The online version of this article offers supplementary material (https://doi.org/10.1515/nanoph-2019-0459).